Tellus (2001), 53B, 491–509
Printed in UK. All rights reserved

TELLUS
ISSN 0280–6509

Development of particle size and composition distributions with a novel aerosol dynamics model

By LIISA PIRJOLA* and MARKKU KULMALA, *Department of Physics, University of Helsinki, PO Box 64, FIN-00014 Helsinki, Finland*

(Manuscript received 11 May 2000; in final form 9 April 2001)

ABSTRACT

An aerosol dynamics model, AEROFOR2, is developed in the context of the BIOFOR project focussing on boreal forest aerosol. It is the second version of a Lagrangian type box model AEROFOR for investigating the formation and growth of particles under clear sky atmospheric conditions. Particles can consist of soluble and insoluble material and the particle population can be externally or internally mixed. AEROFOR2 includes gas phase chemistry and aerosol dynamics, and calculates the number and composition distributions of particles as functions of time. Observed growth rates of the nucleation mode particles after a typical nucleation event are 2–3 nm/h. The model simulations predict that $3 \cdot 10^7$ molecules cm^{-3} of insoluble organic vapour and less than $6 \cdot 10^6$ molecules cm^{-3} of soluble vapour condensing onto particles are enough to make them grow in good agreement with the observed growth rates. Then the source rate of the organic vapour must be an order of 10^5 molecules $cm^{-3}\,s^{-1}$, and its saturation vapour density should be below 10^6 molecules cm^{-3}. If the aerosol was initially an internal mixture of soluble (70%) and insoluble (30%) constituents it transformed to an externally mixed aerosol during the simulation. By applying the externally-mixed aerosol based on measured soluble volume fractions, it was concluded that the modelled soluble fraction of the nucleation mode was too low in comparison with the measurements, and thus, a part of the condensable organic vapour must be water soluble.

1. Introduction

Long-term field measurements of atmosphere-surface interactions have been carried out continuously at the boreal forest measurement station SMEAR II (Station for Measuring forest Ecosystem — Atmosphere Relations) at Hyytiälä, Southern Finland 61°51′N, 24°17′E since the beginning of 1996 (Vesala et al., 1998). Besides meteorological parameters, gas concentrations (e.g., O_3, SO_2, NO, NO_x, H_2O and CO_2), aerosol size distributions and fluxes are measured. The submicron aerosol number distribution is measured inside the 13 m canopy at a height of 2 m. The measurement is performed by a twin DMPS system which is able to detect particles with diameters between 3 nm and 500 nm. The lowest detectable particle concentration in the sub 10 nm range is in the order of 50–100 particles/cm^3 per channel (Mäkelä et al., 2000). One measurement cycle for the whole size range is 10 min.

Bursts of new particle production and the subsequent growth to Aitken mode, or sometimes even to accumulation mode sizes, have been seen regularly on about 50 days in a year. To determine formation mechanisms of aerosol particles at the boreal forest site, and to quantify the amount of condensable vapours produced in photochemical reactions of biogenic volatile organic compounds (BVOC) leading to aerosol formation, a large field campaign BIOFOR (Biological Aerosol

* Corresponding author.
e-mail: liisa.pirjola@helsinki.fi

Formation in the Boreal Forest) was established and performed in three periods during 1998–1999 (Kulmala et al., 2001a). During the campaign, the atmospheric concentrations and emissions of natural hydrocarbons such as isoprene and monoterpenes as well as the composition of particles and their hygroscopic properties were measured. The results indicate that a substantial part of the particle growth is due to condensation of secondary organic material from the oxidation of terpenes (Janson et al., 2001). The growth factor measurements show that particles include both soluble and insoluble material and their composition changes during the day (Hämeri et al., 2001).

Typically, the condensable species are thought to be organic vapours, which can be soluble or insoluble, nonvolatile, semivolatile or highly volatile. However, in other studies, only about 10% of the organic aerosol mass has been identified (Saxena and Hildemann, 1996) and the majority of identified organics are semivolatile or highly volatile (Hoffmann et al., 1998; Griffin et al., 1999; Jang and Kamens, 1999) and thus do not contribute to rapid growth of particles. Model calculations by Kulmala et al. (1998a) and Kerminen et al. (2000) suggest that the growth of nanometer size particles to CCN sizes requires the presence of condensing compounds of extremely low volatility.

The need to study multicomponent condensation and particle hygroscopic properties was a driving force in developing a new version of the aerosol model AEROFOR (Pirjola, 1999) called AEROFOR2. This sectional model includes gas-phase chemistry together with clear-sky photochemical reactions, homogeneous binary H_2SO_4–H_2O or ternary H_2SO_4–H_2O–NH_3 nucleation, multicomponent condensation of H_2SO_4, H_2O and insoluble or soluble organic species, coagulation and dry deposition. In AEROFOR, it was also possible to follow the particle size distribution as a function of time but all particles have the same composition, namely H_2SO_4–H_2O. Now, in AEROFOR2 there are different composition classes for soluble, weakly soluble and insoluble particles. This allows us to follow both the number and composition distributions as well as the total number concentration and the average composition during the simulation.

The aim of this study is to answer the following questions: (1) How much organic vapour is needed and what source rate is required to explain the observed particle growth after a typical nucleation event? (2) How realistic is the assumption that the condensing organic vapour is insoluble (hygroscopic growth factor of unity) and non-volatile? (3) If the pre-existing particle population is internally mixed, how long does it take to be changed to an external mixture. We also study the sensitivity of the results to variations in the equilibrium vapour density of the organics, the water uptake of organic particles, condensation and coagulation sinks and precursor gas concentrations.

2. Model description

AEROFOR2 (Fig. 1) is a development of the Lagrangian type box model AEROFOR (Pirjola, 1999) which simulates the formation and growth of particles under clear sky atmospheric conditions. In AEROFOR2 particles can consist of soluble and insoluble material and the particle population can be externally or internally mixed. AEROFOR2 includes gas phase chemistry and aerosol dynamics, and calculates the number and composition distributions of particles as functions of time. Meteorological data (hourly values of temperature, relative humidity, and mixing height) are typically obtained from trajectories, e.g., calculated from the long-range transport model TRADOS (Valkama et al., 1995) driven by numerical meteorological forecasts provided by the Nordic HIRLAM weather prediction model.

The processes that are included in the model are: (1) emissions of gases, (2) chemical reactions

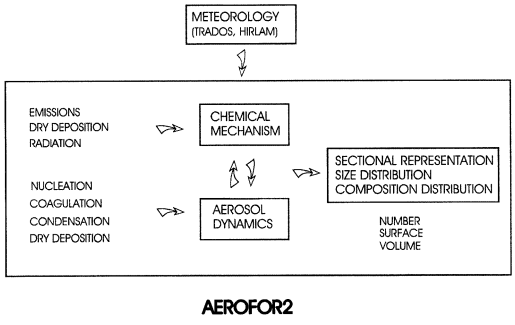

Fig. 1. Schematic diagram of the Lagrangian model AEROFOR2.

in the gas phase, (3) dry deposition of gases, (4) homogeneous binary H_2SO_4–H_2O or ternary H_2SO_4–H_2O–NH_3 nucleation, (5) multicomponent condensation of H_2SO_4, H_2O and some organic vapour onto particles, (6) inter- and intramode coagulation of particles, and (7) dry deposition of particles.

The aerosol size and composition are represented using (nclass1 × nclass2) sections, the first index referring to the size class and the second to the composition class. In this work, we have used 27×9 sections but also 9×5 and 9×21 sections are used for comparison. Naturally the computer time sets the limit for the number of sections. Size classes are evenly distributed on a logarithmic scale; the smallest size is 1 nm and the largest is optional up to 10 μm. Each size class is considered as a monodisperse and all particles which belong to this class have a fixed sum of soluble and insoluble molecules. The composition of particles can be prescribed by the user. For example, if $n$class2 = 11, in the first composition class particles can consist 100% of soluble material (in this study pure sulphuric acid–water), in the next one 90% of soluble and 10% of insoluble, etc. until in the last class they can be pure insoluble particles (i.e., organics or soot).

2.1. Gas-phase chemistry

The chemistry mechanism is based on EMEP (Simpson, 1992). It includes 68 compounds (inorganic and organic) with 140 chemical and photochemical reactions (Pirjola and Kulmala, 1998) and is applicable to simulate rural, urban and marine conditions. The initial concentration, emission rate and deposition velocity of each compound are given to the model as input.

2.2. Nucleation

The binary H_2SO_4–H_2O nucleation rate I is determined using the revised classical nucleation theory (Wilemski, 1984), which is thermodynamically correct, and taking into account the hydrate formation (Jaecker-Voirol et al., 1987). This form of the theory predicts homogeneous nucleation in the sulphuric acid-water system rather well at around 298 K and at relative humidities of 30–50% (Viisanen et al., 1997). To save computer time, we have used a parameterised value for the sulphuric acid mole fraction of the critical nucleus as a function of temperature, relative humidity and relative acidity as described by Kulmala et al. (1998b).

However, several field measurements indicate that observed ambient nucleation rates substantially exceed those predicted based on binary H_2SO_4–H_2O nucleation (Covert et al., 1992; Weber et al., 1998, 1999; Clarke et al., 1999; O'Dowd et al., 1998; O'Dowd et al., 1999). Recently developed classical theory of ternary H_2SO_4–NH_3–H_2O nucleation (Korhonen et al., 1999) predicts that if the NH_3 concentration is over 100 ppt at an H_2SO_4 concentration of 10^6 molecules cm^{-3} significant nucleation can occur. On the other hand, when the H_2SO_4 concentration exceeds 10^7 molecules cm^{-3}, around 20 ppt NH_3 is needed for significant nucleation. However, these results depend on temperature. A preliminary parameterisation for ternary nucleation rate is used in AEROFOR2.

2.3. Condensation

The condensation of H_2O is accounted for by assuming the particles (only soluble part of material) to be in equilibrium with the ambient water vapour. Organic vapour is assumed to be insoluble or water-soluble (Saxena and Hildemann, 1997; Virkkula et al., 1998; Dick et al., 2000).

The molecular flux of the condensing sulphuric acid and organic vapour depends on the difference between the vapour concentration far from the particle (N_a) and at the particle surface ($N_{a,r}$), and on the condensation sink due to the pre-existing particles. It should be noted that under tropospheric conditions saturation vapour pressure of sulphuric acid is much lower than the ambient vapour pressure so its evaporation is negligible. Depending on its saturation vapour pressure, an organic vapour can be nonvolatile ($N_{a,r} = 0$), semivolatile or highly volatile. Because the condensable organic vapour is not identified its thermodynamical properties are not well defined. When considering the saturation vapour pressure; the Kelvin effect due to the curvature of the surface of the particle is taken into account.

The concentration of the condensing vapour N_a is determined by

$$\frac{dN_a}{dt} = Q_a - 4\pi D \sum_{i=1}^{n1} \sum_{j=1}^{n2} \beta_{ij} r_{ij} N_{ij} \times \left[N_a - N_{a,0} \exp\left(\frac{2\sigma M_a}{kT\rho r_{ij}} \right) \right], \quad (1)$$

where Q_a is the net effect of production and loss processes in the gas phase, D is the diffusion coefficient and β_{ij} is the transitional correction factor. $N_{a,0}$ is the saturation vapour density above the solution surface, σ is the surface tension (assumed to be 0.03 kg s^{-2} in this work), M_a the molecular mass (in this work $1.64 \cdot 10^{24}$ kg), ρ the density of the liquid (in this work 1000 kg m^{-3}) and r_{ij} the radius of the particle. The molecular mass and volume has only a minor effect on the condensation rate (Kulmala et al., 1998a) but may have a major effect on the mass fraction of soluble and insoluble material in particles. However, to study those effects is out of the scope of this work. If $N_{a,0} = 0$ the second term on the right hand side of eq. (1) reduces to the condensation sink CS defined below (see also Pirjola et al., 1999). The sums are taken over the size and composition classes:

$$CS = 4\pi D \sum_{i=1}^{n1} \sum_{j=1}^{n2} \beta_{ij} r_{ij} N_{ij}. \quad (2)$$

In the transitional regime CS is between the first and second moments of the size distribution. The transitional correction factor (Fuchs and Sutugin, 1970) is

$$\beta_{ij} = \frac{Kn + 1}{0.377Kn + 1 + \frac{4}{3}\alpha^{-1} Kn^2 + \frac{4}{3}\alpha^{-1} Kn}, \quad (3)$$

where α is the sticking coefficient which we assume to be unity in accordance with the theoretical arguments of Clement et al., 1996. The Knudsen number is $Kn = \lambda_v / r_{ij}$ where the mean free path of vapor molecules, λ_v, is connected to the diffusion coefficient through

$$\lambda_v = 3 \sqrt{\frac{\pi M_v}{8kT}} D. \quad (4)$$

M_v is the molecular mass of the condensing vapour. The molecular diffusion coefficient D can be estimated using an empirical correlation (Reid et al., 1987).

Condensation onto particles in section (i, j) makes them grow, and depending on the amount of condensing vapours, their composition remains the same or changes to a more soluble or to a more insoluble direction. All particles are moved to the section which corresponds to their new size and composition, and if such a section does not exist then the particles are partitioned to the four nearest sections so that the number and mass are conserved. This is presented in Fig. 2a.

2.4. Coagulation

Brownian coagulation coefficients $K_{ij,i'j'}$ between particles in sections (i, j) and (i', j') are calculated according to Fuchs (1964). If particles in section (i, j) coagulate, the number concentration of particles in this section decreases. On the other hand, if two particles collide and the resulting particle has exactly the same size and composition than particles in section (i, j) the particle is allocated to this section. If the composition of the new particle is between the compositions of classes $j-1$ and $j+1$ and the size is between the sizes of classes $i-1$ and $i+1$, partitioning to the four nearest sections is needed. Fig. 2b shows all the cases when the number concentration of section (i, j) increases. It should be noted that a special treatment is needed for size classes $i = 1$ and $i = n$class1 and for composition classes $j = 1$ and $j = n$class2. Particle redistribution caused by condensation and coagulation processes are done simultaneously. Number and mass balances are valid the error being less than 0.1% with a timestep of 600 s.

The coagulation sink for 1 nm particles is defined to be the scavenging rate of these particles to larger ones. It has the expression (Kulmala et al., 2001b)

$$\text{Coag } S = \sum_{i=1}^{n1} \sum_{j=1}^{n2} K_{11,ij} N_{ij}, \quad (5)$$

where $K_{11,ij}$ refers to the coagulation coefficient between a 1-nm particle and a particle in section (i, j) and N_{ij} is the number concentration of particles in section (i, j).

2.5. Dry deposition

Dry deposition rates of particles are modelled according to Schack et al. (1986). Brownian diffusion, interception and gravitational settling are taken into account.

The set of stiff differential equations was solved

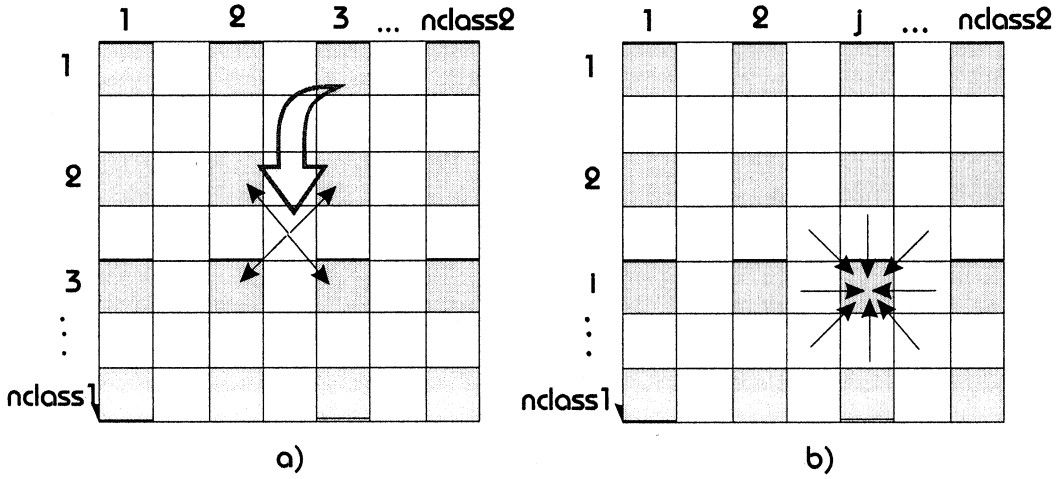

Fig. 2. (a) Partitioning of aerosol particles in the condensation process. Size classes go downwards from 1 to *n*class1 and composition classes to right from 1 (completely soluble) to *n*class2 (completely insoluble). Shadowed areas show the acceptable locations for particles in the model. (b) In the coagulation process, the number and mass concentration of particles in size bin (i, j) increases if the new size and composition of two colliding particles are exactly the same as bin (i, j) has or they are between the nearest bins. In the latter case partitioning determines the amount that is moving to (i, j).

using Numerical Algorithms Group, Ltd. (1990) library FORTRAN-routine D02EJF (1990).

3. Background for the simulations

In the present work, we simulate the particle growth after the nucleation burst and investigate the size distribution and composition of particles. Our purpose is to increase the knowledge about condensing vapours by studying their amounts, mutual ratios and soluble/insoluble properties. As a background, we give a short summary of a range of conditions measured during BIOFOR.

3.1. Typical values

Analyses of observations from several field studies suggest that the ambient sulphuric acid concentrations are not sufficient to make the particles grow to observed sizes (Weber et al., 1998; Kulmala et al., 1998a; O'Dowd et al., 1999; Kulmala et al., 2000a), so an extra condensable vapour, organic or inorganic, is needed. The BIOFOR-data indicate that a substantial part of the growth ought to have been due to condensation of secondary organic material from the oxidation of terpenes (Janson et al., 2001). Sulphuric acid and ammonia are involved in the ternary nucleation mechanism which seems to be the most probable formation mechanism at Hyytiälä (Kulmala et al., 2001a). During the BIOFOR campaign, the measured concentrations of the precursor gases varied from about 10 ppt to 2 ppb for sulphur dioxide and from about 20 ppt to 600 ppt for monoterpenes in daytime with α-pinene accounting for half of them (Janson et al., 2001; see also Kulmala et al., 2000b). The ammonia concentrations ranged from 5 to 400 ppt.

The particle size distribution can be characterised by the condensation sink CS (eq. (2)) and the coagulation sink Coag$S$ (eq. (5)). At Hyytiälä, the condensation sink and the coagulation sink for 1 nm particles vary between 10^{-2} to 10^{-4} s^{-1}, the coagulation sinks being typically half or two over three of the condensation sinks (Kulmala et al., 2001b). As an example, the bimodal lognormal parameters corresponding to Coag$S$ = 10^{-2} s^{-1} could be $N_{\mathrm{Ait}} = 500$ cm^{-3}, $d_{\mathrm{Ait}} = 20$ nm (geometric diameter), $\sigma = 1.46$ (geometric standard deviation) for the Aitken mode and $N_{\mathrm{acc}} =$ 10 cm^{-3}, $d_{\mathrm{acc}} = 130$ nm, $\sigma = 1.45$ for the accumulation mode. Respectively, $N_{\mathrm{Ait}} = 700$ cm^{-3}, $d_{\mathrm{Ait}} =$ 30 nm, $\sigma = 1.46$ and $N_{\mathrm{acc}} = 200$ cm^{-3}, $d_{\mathrm{acc}} =$

130 nm, $\sigma = 1.45$ produce the coagulation sink of $10^{-3}\ s^{-1}$ for 1-nm particles.

Hygroscopic properties of particles were measured during BIOFOR campaigns by two TDMAs (Tandem Differential Mobility Analyser). UF-TDMA (UF stating for ultrafine) was used to study dry particle diameters 10, 15 and 20 nm (nucleation mode), and H-TDMA (H refering to humidity) to study dry diameters 20, 35, 73, 109, 166, 264 and 365 nm of Aitken and accumulation mode particles (Hämeri et al., 2001).

The soluble volume fraction of particles can be estimated from the equation (Pitchford and McMurry, 1994)

$$\varepsilon = \frac{(GF_a^3 - 1)}{(GF_s^3 - 1)}, \quad (6)$$

where GF_a is the growth factor of the ambient particle and GF_s is the growth factor of a fully soluble particle with the same dry diameter as the ambient particle. In the following calculations as well as in the experimental results, the soluble particle is assumed to be ammonium sulphate.

A diurnal pattern of the particle growth factor and solubility was observed (Hämeri et al., 2001). The lowest growth factors ($\sim$1.12–1.17 on average) were detected during late evening and early morning and the maximum ones ($\sim$1.35–1.59 in average) were observed during afternoon. The increase in hygroscopic growth factors started systematically 2–4 h before the nucleation burst was observed. The highest soluble fractions were determined for nucleation mode particles (Hämeri et al., 2001).

3.2. *Case study: 6 April 1999*

A typical nucleation event day, 6 April 1999, during the BIOFOR campaign was selected for a more detailed analysis. As shown in Fig. 3, the total aerosol background concentration is around $3000\ cm^{-3}$. A burst of newly formed particles starts at 11 am and takes 2.5 h raising the aerosol concentration up to $7000\ cm^{-3}$. The number concentration is reduced by coagulation so that 5000 particles cm^{-3} are left at 3 pm just before a pollution burst of larger particles arrives (not considered in this study, since our aim was to study the nucleation mode growth after particle formation). The nucleation mode particles start to grow by condensation and coagulation with the average growth rate 2 nm/h reaching the Aitken mode size in 12 h (Kulmala et al., 2001b).

The simulation time was chosen to be 5 h from 2 pm to 7 pm after the particle formation burst. Hourly values of the temperature, relative humidity, NO, NO_x, O_3, SO_2, and α-pinene concentrations were adopted from the measurements (Fig. 4) as well as the initial concentrations of β-pinene (12 ppt), 3-carene (56 ppt) and d-limonene (9 ppt) (see also BIOFOR homepage).

The size distribution measurements by DMPS provided lognormal fittings with 3 modes at 2 pm: $N_{nuc} = 2915\ cm^{-3}$, $d_{nuc} = 10$ nm and $\sigma_{nuc} = 1.3$ for the nucleation mode, $N_{Ait} = 999\ cm^{-3}$, $d_{Ait} = 56$ nm and $\sigma_{Ait} = 1.9$ for the Aitken mode, and $N_{acc} = 244\ cm^{-3}$, $d_{acc} = 160$ nm and $\sigma_{acc} = 1.6$ for the accumulation mode. The calculated sinks are then $CS = 3.6 \cdot 10^{-3}\ s^{-1}$ and $CoagS = 2.7^{-3}\ s^{-1}$ for 1 nm particles.

For the nucleation mode particles the measured growth factors showed maximum values at noon-afternoon (1.3–1.36) and the calculated soluble fractions were between 50–60% (20 nm particles) and 70–80% (10-nm particles) (Hämeri et al., 2001). At 2 pm, GF_a for 10-nm particles was 1.27 ($RH = 91.4\%$). At the same time the measured growth factor of ammonium sulphate GF_s was 1.36 thus giving the result of 0.69 for the soluble volume fraction. The corresponding values 2.5 h later for 15 nm particles were 1.31 and 1.47, respectively, and the estimated soluble volume fraction was then about 0.57. During that time 10 nm particles have grown to 15 nm size (Kulmala et al., 2001b) and we can conclude that in the nucleation mode the amount of soluble material has decreased from 69% to 57%. The growth factors for 15–20 nm particles were almost constant during the next couple of hours. For the Aitken mode particles, the soluble volume fraction was approximately 0.4 at 2 pm and then decreased to about 0.3 until 7 pm. The accumulation mode particles were characterised by the more hygroscopic particles with GF_a between 1.4–1.65 and the less hygroscopic particles with GF_a between 1.0–1.25. The soluble volume fractions were about 0.2 and 0.8 at 2 pm and 0.15 and 0.7 at 7 pm.

4. Results and discussion

As a first approximation, we assumed that the condensable organic vapour X is insoluble and

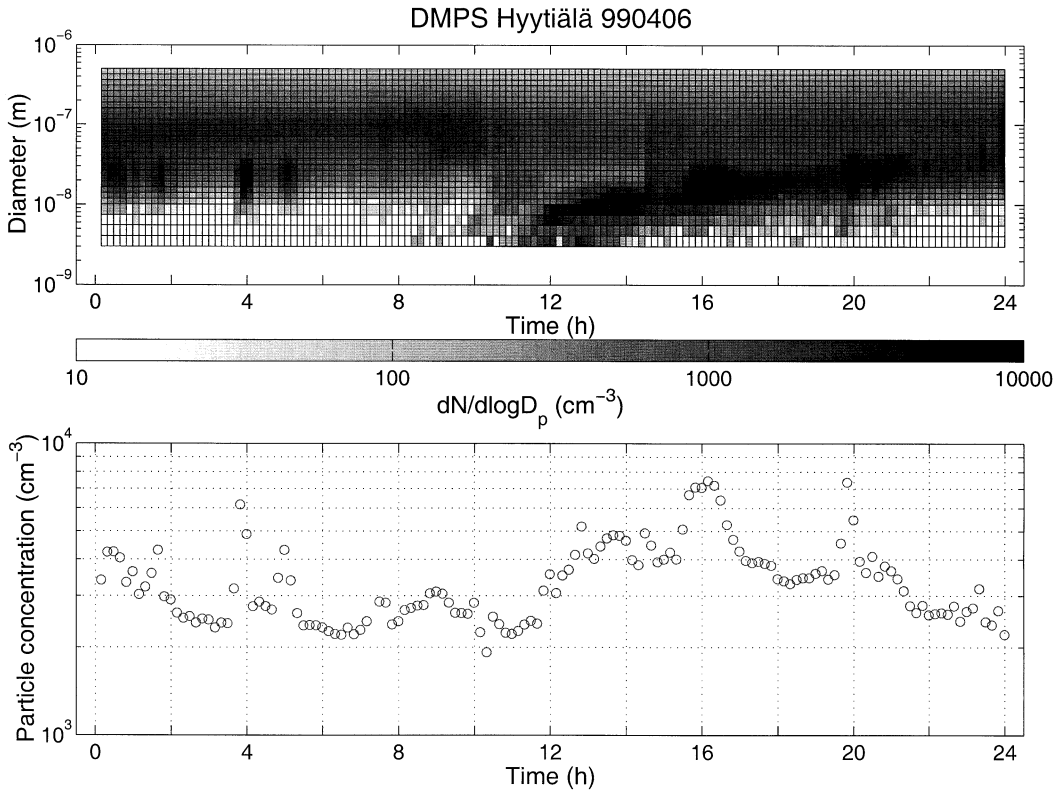

Fig. 3. The development of the measured particle size distribution and particle number concentration at Hyytiälä, Finland, on 6 April 1999. X-axis refers to the day of the year, y-axis to the particle diameter (upper figure) and colour indicates 10-min average number concentration of particles in each size bin.

non-volatile. X is assumed to be formed from α-pinene so that the production rate of X is 15% of the chemical loss reaction rates of α-pinene (i.e., α-pinene + OH, α-pinene + O_3 and α-pinene + NO_3). The condensation of X onto pre-existing particles is taken into account as explained in Section 2. Since the measurements of OH and H_2SO_4 concentrations were not available during the BIOFOR project the chemistry mechanism in the model predicts the OH, NO_3 and H_2SO_4 concentrations as a function of time under clear sky conditions.

The simulated concentrations of H_2SO_4 and X are plotted in Fig. 5. The H_2SO_4 concentration is relatively low and it decreases from $5.4 \cdot 10^6$ to $1.2 \cdot 10^5$ molecules cm^{-3} during the simulation time. The reason for this can be found by considering the precursors of H_2SO_4: the SO_2 concentration is moderately low, below 1 ppb, and the OH concentration has a diurnal cycle with a maximum at noon, decreasing strongly in the afternoon (from $1 \cdot 10^6$ molecules cm^{-3} at 2 pm to $3.3 \cdot 10^4$ molecules cm^{-3} at 7 pm). Janson et al. (2001) calculated the steady state OH concentrations and found that average noon values were $(3 \pm 1) \cdot 10^6$ molecules cm^{-3} on event days. The concentration of X follows the changes of the α-pinene concentration; first X decreases from $2.4 \cdot 10^7$ to $1.2 \cdot 10^7$ molecules cm^{-3} and then towards the evening X enhances up to $4.0 \cdot 10^7$ molecules cm^{-3}. The source rate of X has the same pattern as the concentration of X with the minimum value of $4.6 \cdot 10^4$ and the maximum value of $1.5 \cdot 10^5$ molecules cm^{-3} s^{-1}. If the source rate of X was less than 15% of the α-pinene loss rate then the modelled particle growth rate was too small. Similarly, if the source rate was larger than 15%, the modelled growth rate was too large

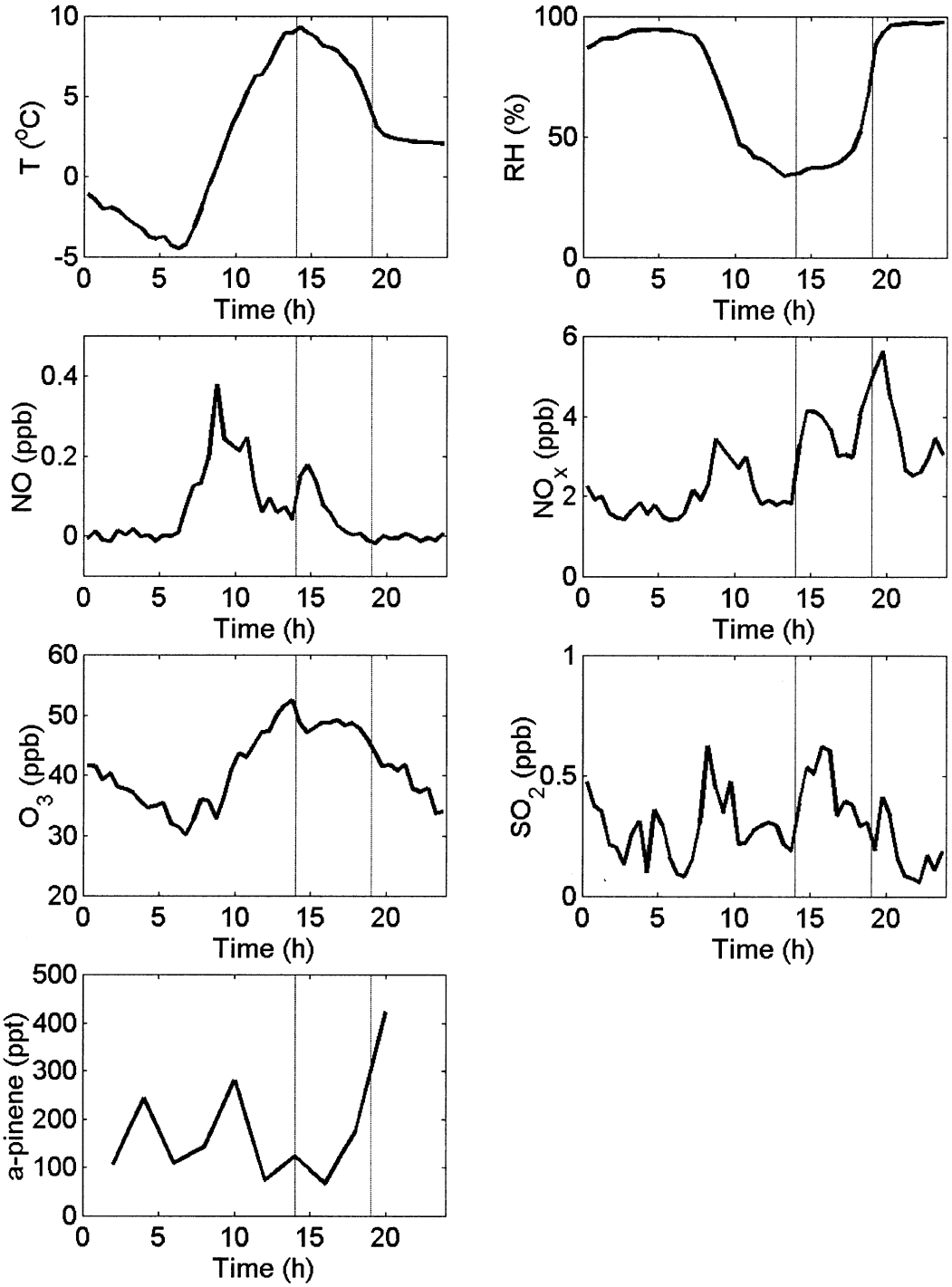

Fig. 4. Measured values of temperature, relative humidity, NO, NO_x, O_3, SO_2 and α-pinene concentrations at Hyytiälä on 6 April 1999. The modelled simulation time is between the vertical lines.

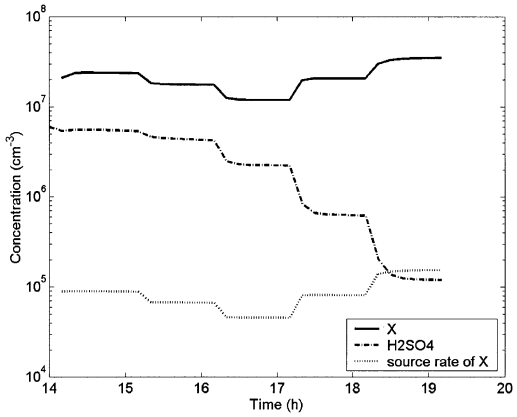

Fig. 5. Modelled concentrations of sulphuric acid and insoluble organic vapour X. Also the source rate of X ($cm^{-3}\,s^{-1}$) is plotted.

compared to the inferred growth rate for the nucleation mode of 2 nm/h (assuming that the pollution burst was a temporary disturbance of an otherwise homogeneous air parcel) suggesting that this is an appropriate value. Janson et al. (2001) and Kulmala et al. (2001b) came to the same result from their calculations based on measurements. Moreover, this result is in a good agreement with our recent calculations presented by Kulmala et al., 2000a.

4.1. Internally mixed aerosol

We have performed two separate simulations where different compositions for the particle population were used. First, we have assumed that at the beginning of the simulation all particles have the same composition, i.e., the aerosol is internally mixed. When used 9 size sections and 5 composition classes (100, 75, 50, 25 and 0% soluble material) all the particles included 75% of soluble and 25% of insoluble organic material, the nearest composition class as compared to the measured value (69%). By using 27 size sections and 9 composition classes (80, 70, 60, 50, 40, 30, 20, 10, and 0% soluble material) all particles included 70% of soluble, and 30% of insoluble, material. It should be noted that in this case, inclusion of composition classes containing more than 80% soluble species are not needed because the concentration of condensable organic vapour is much higher than the sulphuric acid concentration and thus the composition can change only to the direction of less soluble. This simulation is thereafter called as a base case.

Fig. 6a,b illustrates the initial and final size distributions for 9×5 sections (a) and for 27×9 sections (b). At the beginning of the simulation all particles had the same composition but 5 h later, there were particles possessing different compositions and therefore the aerosol is changed to externally mixed. Because condensation to large particles changes the mass slowly, the major part of the accumulation mode particles remain in their original composition class (75% of soluble in (a) and 70% of soluble in (b)). The smaller the particles are, the more they grow by condensation, and due to the higher insoluble organic flux, the less soluble they become. Thus smaller particles include more organic material than larger ones. Numerical diffusion which is typical for sectional representation with a small number of size sections is also present in the composition distributions. The reallocations of particles to the four nearest sections in condensation and coagulation overestimates the mass in the 0% soluble class. The less composition classes the stronger the effect. However, the influence of numerical diffusion on the average modal mass-weighted composition is not significant. When the number of composition classes changed from 5 to 21 the average mass-weighted soluble fraction of the nucleation mode varied only between 0.24 and 0.29, and the variations for the Aitken and accumulation modes were really small.

Figs. 6c,d show the time development of the total average composition and the average compositions in each mode. Particles with dry diameter in the range of 1–20 nm are classified to the nucleation mode, 20–100 nm to the Aitken mode and 100 nm–2 μm to the accumulation mode. In Fig. 6c, the average composition refers to the soluble fraction weighted by the number concentration. The soluble fraction of the nucleation mode changes from 70% to 22% whereas the Aitken mode soluble fraction decreases down to 45% at 7 pm. Due to the small number concentration of the accumulation mode the total composition is determined mainly by the composition of smaller particles and its final value is 35%. In comparison, Fig. 6d depicts the mass weighted average soluble fraction. The composition of the smallest particles (nucleation mode) again changes

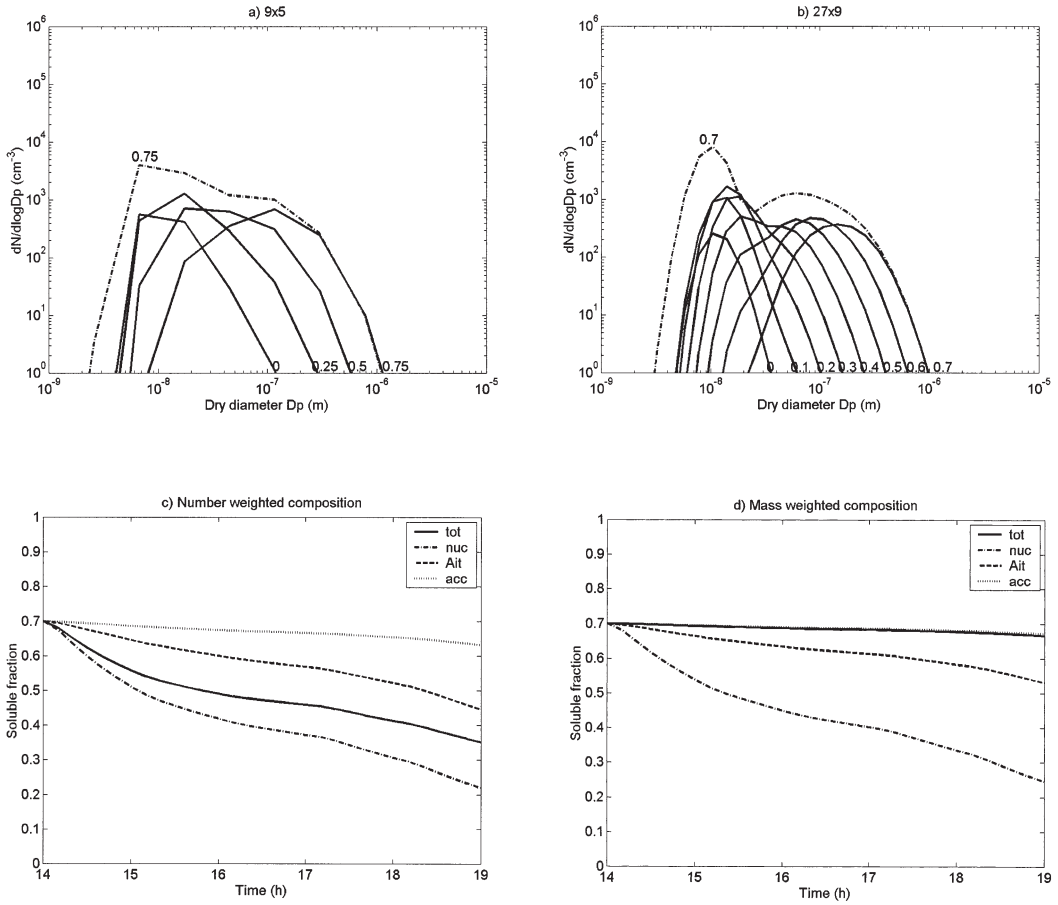

Fig. 6. The particle size distributions at 2 pm (dashdot) and at 7 pm (solid) with 9×5 and 27×9 sections. At the beginning aerosol was internally mixed and all particles included 75% soluble and 25% insoluble organics (a) or 70% soluble and 30% insoluble (b). Marked composition refers to the soluble fraction. The average total and modal number weighted (c) and mass weighted (d) compositions are plotted as functions of time.

dramatically to the organic direction (down to 0.24 at 7 pm) whereas the larger particles, which in practice affect mostly the mass, remain in their original composition class. The difference between total number and mass weighted soluble fractions are larger and therefore more worthy of noting. In both figures the effect of the increase of the ambient organic vapour concentration after 5 pm is seen.

4.2. *Externally mixed aerosol*

Secondly, the aerosol is assumed to be externally mixed and the initial soluble volume fractions in each mode are estimated according to the measurements. Consequently, nucleation mode particles include 70% of soluble and 30% of insoluble organics, Aitken mode particles 40% of soluble and 60% of insoluble, and half of the accumulation mode particles include 20% of soluble and 80% of insoluble and the other half vice versa. This simulation was carried out only by 27×9 sections.

Fig. 7 shows the time development of the particle size distribution when the aerosol is assumed to be externally mixed. The lognormal fittings based on the measurements are used to obtain the initial lognormal parameters of the different modes, and the soluble fraction of each mode is

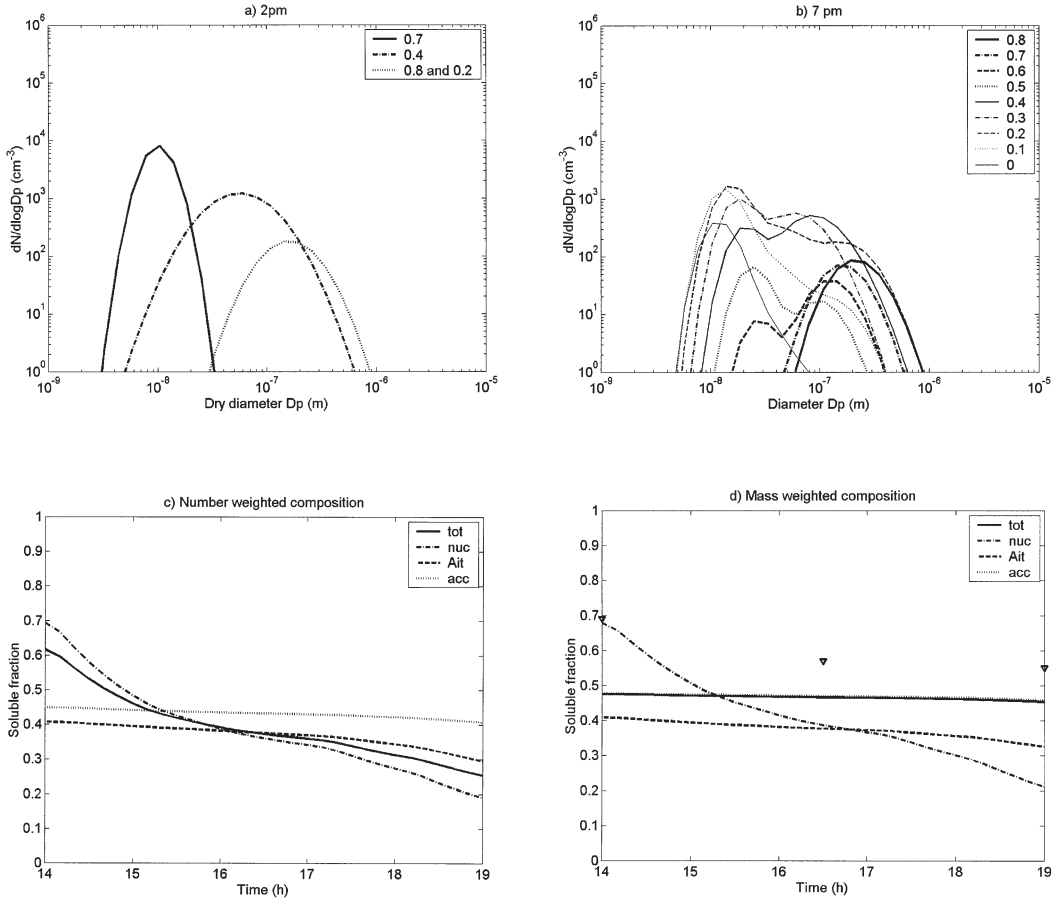

Fig. 7. The particle size distributions at 2 pm (a) and at 7 pm (b) with 27 × 9 sections. At the beginning aerosol was externally mixed and the nucleation mode particles include 70%, Aitken mode particles 40% and half of the accumulation mode particles 80% and the other half 20% (curves coincide) of soluble and the rest of insoluble organics. The average total and modal number weighted (c) and mass weighted (d) compositions as functions of time. The triangles in figure (d) denote the soluble fractions of the nucleation mode based on the measurements.

chosen as explained above. At 2 pm, the geometric standard deviations (GSD) for the Aitken and accumulation modes were as large as 1.9 and 1.6 and this caused the modes to overlap greatly (Fig. 7a). Consequently, the major part of the particle population had at least a bimodal composition structure. After 5 h, more composition classes have appeared and almost all of them covered a wide diameter range. The time development of the size distribution was compared to the observed ones and the agreement was very good for the smallest particles. However, the observed accumulation mode particles were somewhat bigger due to the pollution burst.

To study in more detail the development of each composition class, we have calculated the composition distribution, normalised to the mode number concentration, for different modes at 2 pm, 5 pm and 7 pm (Fig. 8). At the beginning, all nucleation mode particles included 70% soluble species but due to the large GSD of the Aitken mode and the sectional representation a small part of particles containing 40% of soluble species were included in this mode. With time their composition changed to insoluble organic species due to the higher organic acid concentration compared to the sulphuric acid concentration. After 5 h, the average soluble fraction was somewhat less than

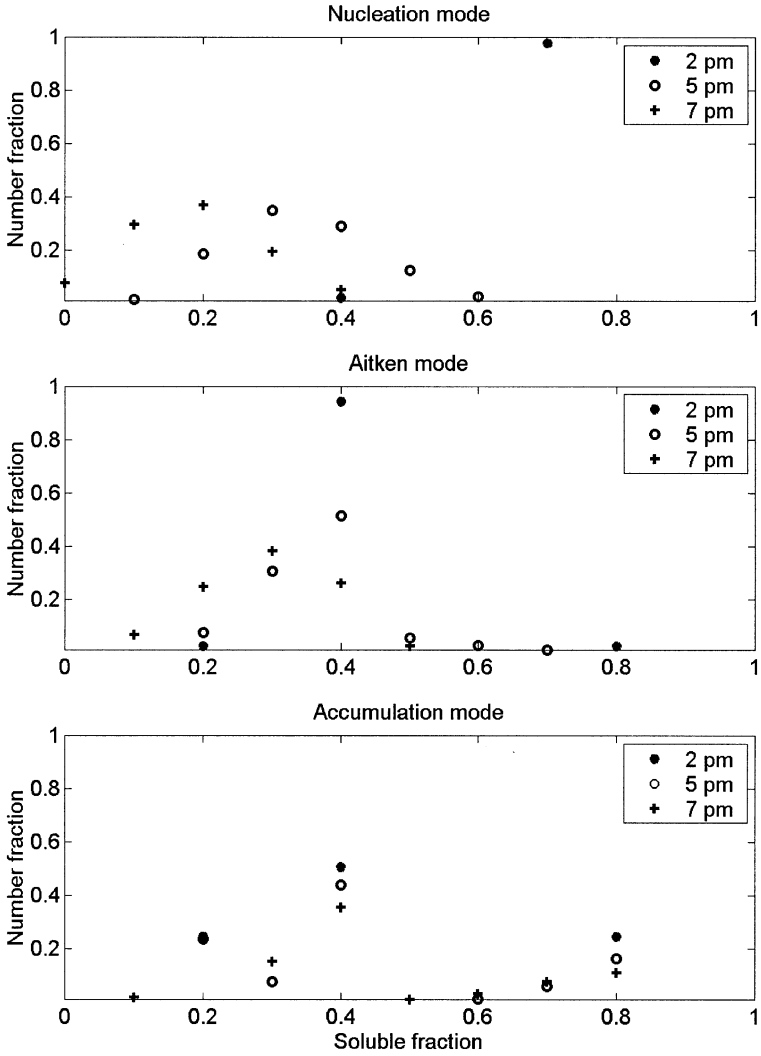

Fig. 8. Time evolution of the composition in each mode. X-axis refers to the soluble fraction and *y*-axis to the number fraction.

20%. Initially, Aitken mode particles included 40% of soluble species but a small part of the accumulation mode particles with 80% and 20% of soluble material. The composition changed towards a more insoluble direction so that after 5 h, the average soluble fraction was about 30%. The accumulation mode particles had a bimodal composition, half of them contained 80%, and the other half, 20% of soluble species. But again the tail of the Aitken mode caused a 3rd composition class to appear, so initially 50% of particles contained 40% of soluble species and the rest of the particles were evenly distributed containing 20% and 80% of soluble species. After 5 h, the composition was changed only slightly as was expectable for the same reason as in Fig. 6.

Additionally, the average number and mass weighted compositions for each mode are presented in Fig. 7c,d. Similar conclusions as from Fig. 8 can be drawn. Furthermore, in the number-weighted case the average composition of all particles (curve tot) follows the changes in the nucle-

ation and Aitken modes whereas in the mass-weighted case it naturally follows the composition of the accumulation mode particles. At 7 pm in Fig. 7d, the soluble fraction is about 21% for the nucleation mode particles, 33% for the Aitken mode and about 46% for the accumulation mode particles. The estimated values from the measurements are about 57% for the nucleation mode, about 30% for the Aitken mode, and 15% and 70% for the accumulation mode. The measurements showed that towards the evening, on April 6, the fraction of more hygroscopic particles increased, and at 7 pm it was approximately 60%. At the same time the average accumulation mode composition was about 48% of soluble material.

The model study results in less hygroscopic nucleation mode particles than obtained from the measurements (triangles in Fig. 7d). This disagreement suggests that a part of the condensable organic vapour might be soluble. This is also plausible since 20–70% of organic matter in atmospheric aerosols is water soluble (Saxena and Hildemann, 1996).

4.3. *Nucleation*

We performed some model runs to simulate a typical nucleation event day 6 April. Just before the event at 11 am the pre-existing aerosol possessed two modes in the Aitken size with the log-normal parameters $N_1 = 1529\ \mathrm{cm}^{-3}$, $d_1 = 67$ nm, $\sigma_1 = 2.2$ and $N_2 = 138\ \mathrm{cm}^{-3}$, $d_2 = 83$ nm, $\sigma_2 = 1.2$ causing a condensation sink of $0.0047\ \mathrm{s}^{-1}$ and a coagulation sink of $0.0036\ \mathrm{s}^{-1}$. Based on hygroscopic measurements with H-TDMA, we estimated that the soluble fraction of the smaller Aitken mode particles was 0.2, as well as for a half of the greater particles whereas for the other half it was 0.7. These values were used as input to the model. Meteorological parameters as well as the gas concentrations were adopted from observations as in the base case simulation. The nucleation mechanism was ternary H_2SO_4–H_2O–NH_3 nucleation.

Under these conditions and with the ammonia concentration of 9 ppt the total number concentration (N_{tot}) increased up to about $15000\ \mathrm{cm}^{-3}$. Due to strong coagulation the concentration of detectable particles (diameter > 3 nm) N_3 was only about $2500\ \mathrm{cm}^{-3}$at maximum. However, the observed N_3 was about $5000\ \mathrm{cm}^{-3}$ if the transported pollution peak at 4 pm was not taken into account (Fig. 3). It should be noted that ternary nucleation is very sensitive to the ammonia concentration whose measured value was as high as 40 ppt. By increasing NH_3 to 15 ppt the concentration of newly formed particles enhanced dramatically but at the same time self-coagulation started to consume particles so that after 10 min, N_3 was below $4000\ \mathrm{cm}^{-3}$ at maximum. This indicated that the amount of condensable vapours was not enough to make the new particles grow sufficiently fast. If the source rate of organic vapour X was increased from 15% to at least 200% of the α-pinene loss rate, N_3 was about $4200\ \mathrm{cm}^{-3}$ after 2 h of the start of the nucleation event, and closer to the observations. However, then the source rate of X was more than one order of magnitude higher than the values estimated by Kulmala et al. (2001b). Another possibility to increase condensation is to decrease the condensation sink due to pre-existing particles. Then we can assume that new particle formation occurred not near the earth's surface but at a little bit higher altitudes where the background concentration of existing particles was lower. Flux measurements (Buzorius et al., 1998) and the boundary layer evolution during the late morning from stable, nocturnal conditions to a deep and convective well-mixed boundary layer (Nilsson et al., 2001) support this idea. As a summary, the conditions which favour the formation of N_3 are presented in Table 1.

5. Sensitivity studies

Base case simulations were repeated in order to test the size and composition distributions against the variables such as the equilibrium vapour pres-

Table 1. *Processes which favour the formation of particles with diameter ⩾1 nm (N1) and of detectable particles with diameter ⩾3 nm (N3)*

Process	N1 formation	N3 in agreement with measurements
increase in NH_3	+	−
increase in the source rate of X	−	−
decrease in CS	+	+

sure, the growth factor, the gas phase precursor concentrations and the pre-existing particle population.

5.1. Equilibrium pressure of organic vapour

In the simulations presented above the organic vapour was assumed to be insoluble and non-volatile with the zero saturation vapour density, i.e., the vapour density above the solution surface. Available relevant saturation vapour pressures of secondary organic aerosol compounds vary from a few ppt to several tens of ppb (Tao and McMurry, 1989; Pandis et al., 1991; Jang and Kamens, 1999). However, Kulmala et al. (1998a) found that the saturation vapour density of the condensing vapour should be below 10^5 molecules cm^{-3} to get a growth curve in accord with the measurements at Hyytiälä. Fig. 9 illustrates our results with the saturation vapour density up to 10^8 molecules cm^{-3}. If the vapour density is 10^6 molecules cm^{-3} or more the growth of the particles was slower because of evaporation. This can be clearly observed in the nucleation and Aitken mode particles. From the same reason the composition of the particles in the smaller modes changed to the more soluble direction.

5.2. Organic vapour uptakes water

In the above simulations the organic vapour did not uptake water. To study the sensitivity of the results to this assumption, we assumed that the organic species in the aerosol phase was able to uptake water so that the hygroscopic properties of the particles were determined by both the inorganic and organic compounds. The hygroscopic growth factor was assumed to be 1.1 at RH = 90% for pure organic particles and 1.5 for completely soluble particles. The soluble fraction of pure organic particles was $\sim 14\%$ according to eq. (5). Therefore, the soluble mass of all particles contained, besides the inorganic soluble mass, 14% of their organic mass. The water uptake slightly affected the growth of nucleation and Aitken mode particles and their compositions. Table 2 shows that at the end of the simulation the soluble fraction of the nucleation mode was 30%, almost twice as much as in the base case, and 53% for the Aitken mode.

5.3. Precursor gases

Because the precursor gas concentrations vary independently of each other, we performed four simulations where the measured SO_2 and α-pinene concentrations were both multiplied by 5, both divided by 5, one multiplied by 5 and the other divided by 5 and vice versa. The size distributions are presented in Fig. 10 and mass-weighted compositions in Table 2. Only in the case when SO_2 had a higher concentration than α-pinene, the H_2SO_4 concentration exceeded that of X. During the first hour H_2SO_4 was as high as $1 \cdot 10^8$ cm^{-3} and not until after 3 h dropped below $1 \cdot 10^7$ cm^{-3}. Consequently, the soluble fraction was more than 0.7 except for the nucleation mode (Table 2). When the concentration of the organic vapour was higher it clearly determined the growth rate independently of the H_2SO_4 concentration, and the soluble fraction was really small, especially in the nucleation and Aitken modes.

5.4. Condensation and coagulation sinks

Simulations were repeated by changing the number concentrations of Aitken and accumulation mode particles thus causing changes in the condensation and coagulation sinks. The values used were $N_{ait} = 1000$ cm^{-3} and $N_{acc} = 1200$ cm^{-3} for the first case and $N_{ait} = 100$ cm^{-3} and $N_{acc} = 100$ cm^{-3} for the second case thus covering the typical condensation and coagulation sinks at Hyytiälä (Table 2).

When the total pre-existing aerosol condensation sink was small, condensation growth of the nucleation mode particles proceeded more rapidly than in the base case, and due to the higher organic vapour concentration, they contained almost pure insoluble material. If the condensation sink was higher the particles grew slower, and the composition of the nucleation and Aitken mode particles remained more soluble than in the base case.

6. Conclusion

The developed model AEROFOR2 is a Lagrangian type box model for investigating the formation and growth of particles under clear sky atmospheric conditions. Particles can consist of soluble and insoluble material and the particle

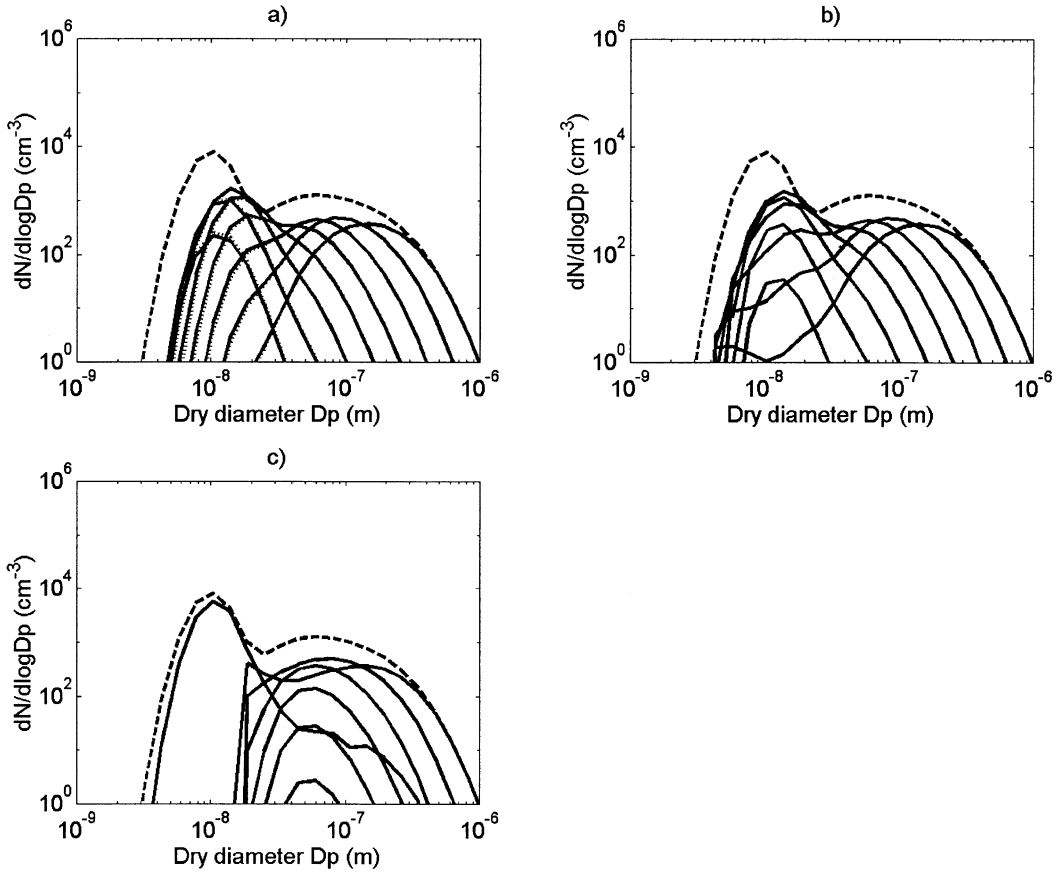

Fig. 9. The particle size distributions at 2 pm (dashdot) and at 7 pm (solid) with the saturation vapour pressure at the particle surface of 10^6 (a), 10^7 (b), and 10^8 molecules cm^{-3} (c). Dotted curves in (a) refer to the cases when the saturation vapour density varies from 0 to 10^5 molecules cm^{-3}. At the beginning aerosol was internally mixed and all particles included 70% of soluble and 30% of insoluble material. The soluble fraction evenly decreases from 0.7 (the curve located to the right) to 0 (the curve located to the left).

population can be externally or internally mixed. AEROFOR2 includes gas-phase chemistry and aerosol dynamics, and calculates the particle number and composition size distributions as functions of time.

Based on measured values of temperature, relative humidity, NO, NO_x, SO_2 and α-pinene concentrations, and by using the lognormal fittings from the measured size distributions, the model estimates the ambient H_2SO_4 concentration to be about $6 \cdot 10^6$ molecules cm^{-3} and insoluble organic vapour, which is formed photochemically from α-pinene, to be about $3 \cdot 10^7$ molecules cm^{-3}. With these vapour concentrations and with the saturation vapour density below $1 \cdot 10^6$ molecules cm^{-3} the particle growth rate nicely followed the observed growth rate of ~ 2 nm/h during the 5-hour simulation from 2 pm to 7 pm on 6 April 1999.

If the aerosol was initially an internal mixture of soluble and insoluble constituents with 70% soluble and 30% insoluble material it was found that during the 5-hour simulation it was changed to externally mixed aerosol. By applying the measured soluble volume fractions for the initial size distributions, i.e., for each mode of the log-normal fitting, the aerosol was externally mixed. Then by following the composition distribution and the average composition of each mode, it was concluded that the modelled nucleation mode soluble

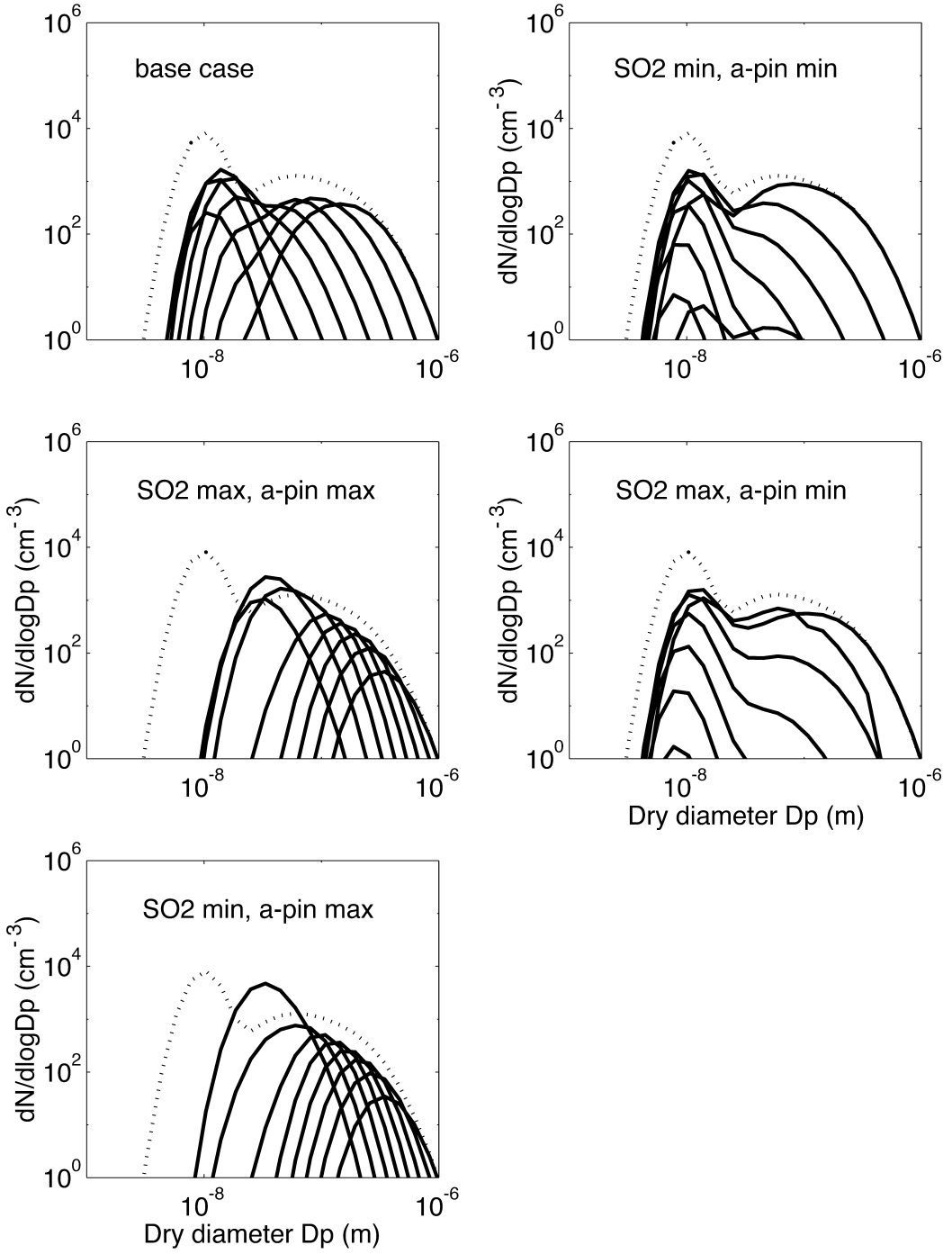

Fig. 10. The particle size distributions at 2 pm (dotted) and at 7 pm (solid) with the different precursor vapour concentrations. At the beginning aerosol was internally mixed and all particles included 70% of soluble and 30% of insoluble material. The soluble fraction decreases from 0.7 (the curve located to the right) to 0 (the curve located to the left). In the subplot where the SO_2 concentration is at maximum and the α-pinene concentration at minimum the pure insoluble curve is missing.

Table 2. *The parameters varied in the 5 h simulation and the compositions at the end of the simulation*

SO_2 (cm^{-3})	X (cm^{-3})	GF	CS (s^{-1})	Coag$S$ (s^{-1})	$N_{a,0}$ (cm^{-3})	SF_{Nucl}	SF_{Ait}	SF_{Acc}	SF_{Tot}
meas	meas	1.0	$3.6 \cdot 10^{-3}$	$2.7 \cdot 10^{-3}$	0	0.24	0.53	0.67	0.67
meas	meas	1.0	$3.6 \cdot 10^{-3}$	$2.7 \cdot 10^{-3}$	10^6	0.24	0.53	0.67	0.67
meas	meas	1.0	$3.6 \cdot 10^{-3}$	$2.7 \cdot 10^{-3}$	10^7	0.32	0.54	0.67	0.67
meas	meas	1.0	$3.6 \cdot 10^{-3}$	$2.7 \cdot 10^{-3}$	10^8	0.79	0.59	0.67	0.67
meas	meas	1.1	$3.6 \cdot 10^{-3}$	$2.7 \cdot 10^{-3}$	0	0.33	0.57	0.67	0.67
meas5	meas5	1.0	$3.6 \cdot 10^{-3}$	$2.7 \cdot 10^{-3}$	0	0.07	0.17	0.53	0.51
meas/5	meas/5	1.0	$3.6 \cdot 10^{-3}$	$2.7 \cdot 10^{-3}$	0	0.55	0.67	0.70	0.69
meas5	meas/5	1.0	$3.6 \cdot 10^{-3}$	$2.7 \cdot 10^{-3}$	0	0.70	0.75	0.71	0.71
meas/5	meas5	1.0	$3.6 \cdot 10^{-3}$	$2.7 \cdot 10^{-3}$	0	0.003	0.07	0.50	0.48
meas	meas	1.0	$1.1 \cdot 10^{-2}$	$0.79 \cdot 10^{-2}$	0	0.46	0.64	0.69	0.69
meas	meas	1.0	$1.0 \cdot 10^{-3}$	$0.68 \cdot 10^{-3}$	0	0.08	0.22	0.63	0.61

$N_{a,0}$ refers to the saturation vapour density of organic species X above the solution surface. SF_{nuc} is the mass weighted soluble fraction in the nucleation, SF_{Ait} in the Aitken and SF_{acc} in the accumulation mode and SF_{tot} altogether. The first row refers to the base case simulation.

fraction was too low as compared to the measurements and thus a part of the condensable organic vapour should be water-soluble. The composition of Aitken and accumulation mode particles was in a better agreement with the measurements.

More work is necessary to further develop the model so that the soluble fraction of the particles and their physical and thermodynamical properties can be better predicted. Also the numerics of the model should be improved.

7. Acknowledgments

This work was supported by the European Union under contracts ENV4-CT98–0405 (BIOFOR). The authors thank the referees for their positive criticism and the many suggestions which significantly improved the manuscript.

REFERENCES

BIOFOR homepage, http://mist.helsinki.fi/Biofor/index.html

Buzorius, G., Rannik, Ü., Mäkelä, J. M., Vesala, T. and Kulmala, M. 1998. Vertical aerosol particle fluxes measured by eddy covariance technique using condensational particle counter. *J. Aerosol Sci.* **29**, 157–171.

Clarke, A. D., Kapustin, V. N., Eisele, F. L., Weber, R. J. and McMurry, P. H. 1999. Particle production near marine clouds: Sulfuric acid and predictions from classical binary nucleation. *Geopfys. Res. Lett.* **26**, 2425–2428.

Clement, F. C., Kulmala, M. and Vesala, T. 1996. Theoretical consideration on sticking probabilities. *J. Aerosol Sci.* **27**, 869–882.

Covert, D. S., Kapustin, V. N., Quinn, P. K. and Bates, T. S. 1992. New particle formation in the marine boundary layer. *J. Geophys. Res.* **97**, 20,581–20,587.

Dick W. D., Saxena P. and McMurry P. H. 2000. Estimation of water uptake by organic compounds in submicron aerosols measured during the South-eastern aerosol and visibility study. *J. Geophys. Res.* **101**, 1471–1479.

FORTRAN-routine D02EAF. 1990. *The NAG Workstation Library Handbook 1*. The Numerical Algorithms Group Ltd., Oxford.

Fuchs, N. A. 1964. *The mechanics of aerosols*. Pergamon Press, London.

Fuchs, N. A. and A. G. Sutugin. 1970. *Highly dispersed aerosols*. Ann. Arbor Science Publ., Ann Arbor, Michigan.

Griffin R. J., Crocker III D. R., Flagan R. C. and Seinfeld J. H. 1999. Organic aerosol formation from the oxidation of biogenic hydrocarbons. *J. Geophys. Res.* **104**, 3555–3567.

Hoffmann T., Bandur R., Marggraf U. and Linscheid M. 1998. Molecular composition of organic aerosols formed in the α-pinene/O_3 reaction: implications for new particle formation processes. *J. Geophys. Res.* **103**, 25,569–25,578.

Hämeri, K., Väkevä, M., Aalto, P., Kulmala, M., Swietlicki, E., Seidl, W., Becker, E. and O'Dowd, C. D. 2001. Hygroscopic and CCN properties of aerosol particles in boreal forests. *Tellus* **53B**, this issue.

Jang M. and Kamens R. M. 1999. Newly characterized

products and composition of secondary aerosols from the reaction of α-pinene with ozone. *Atmos. Environ.* **33**, 459–474.

Janson, R., Rosman, K., Karlsson A. and Hansson, H.-C. 2001. Biogenic emissions and gaseous precursors to forest aerosols. *Tellus* **53B**, 423–440.

Jaecker-Voirol, A., Mirabel, P. and Reiss, H. 1987. Hydrates in supersaturated binary sulphuric acid-water vapor: A reexamination. *J. Chem. Phys.* **87**, 4849–4852.

Kerminen V.-M., Virkkula A., Hillamo R., Wexler A. S. and Kulmala M. 2000. Secondary organics and atmospheric cloud condensation nuclei production. *J. Geophys. Res.* **105**, 9255–9264.

Korhonen, P., Kulmala, M., Laaksonen, A., Viisanen, Y., McGraw, R. and Seinfeld, J. H. 1999. Ternary nucleation of H_2SO_4, NH_3, and H_2O in the atmosphere. *J. Geophys. Res.* **104**, 26,349–26,353.

Kulmala, M., Toivonen, A., Mäkelä, J. M. and Laaksonen, A. 1998a. Analysis of the growth of nucleation mode particles observed in Boreal forest. Tellus, **50B**, 449–462.

Kulmala, M., Laaksonen, A. and Pirjola, L. 1998b. Parameterizations for sulphuric acid/water nucleation rates. *J. Geophys. Res.* **103**, 8301–8308.

Kulmala, M., Pirjola, L. and Mäkelä, M. 2000a. Stable sulphate clusters as a source of new atmospheric particles. *Nature* **404**, 66–69.

Kulmala, M. Rannik, Ü, Pirjola, L., Dal Maso, M., Karimäki, J., Asmi, A., Jäppinen, A., Karhu, V., Korhonen, H., Malvikko, S.-P., Puustinen, A., Raittila, J., Romakkaniemi, S., Suni, T., Yli-Koivisto, S., Paatero, J., Hari, P. and Vesala, T. 2000b. Characterization of atmospheric trace gas and aerosol concentrations at forest sites in southern and northern Finland using back trajectories. *Boreal Environ. Res.* **5**, 315–336.

Kulmala, M., Hämeri, K., Aalto, P. P., Mäkelä, J. M., Pirjola, L., Nilsson, E. D., Buzorius, G., Rannik, Ü, Dal Maso, M., Seidl, W., Hoffmann, T., Janson, R., Hansson, H.-C., Viisanen, Y., Laaksonen, A. And O'Dowd, C. D. 2001a. Overview of the international project on Biogenic aerosol formation in the boreal forest (BIOFOR). *Tellus* **53B**, 327–340.

Kulmala, M. Dal Maso, M., Mäkelä, J. M., Pirjola, L., Väkevä, M., Aalto, P., Miikkulainen, P., Hämeri, K. and O'Dowd, C. D. 2001b. On the formation, growth and composition of nucleation mode particles. *Tellus* **53B**, 479–490.

Mäkelä, J. M., Koponen, I. K., Aalto, P. and Kulmala, M. 2000. Modal structure of number size distribution of ambient submicron particles at a boreal forest site. *J. Aerosol Sci.* **31**, 595–611.

O'Dowd, C. D., Geever, M., Hill, M. K., Jennings, S. G. and Smith, M. H. 1998. New particle formation: Spatial scales and nucleation rates in the coastal environment, *Geophys. Res. Letts* **25**, 1661–1664.

O'Dowd, C. D., McFiggens, G., Pirjola, L., Creasey, D. J., Hoell, C., Smith, M. H., Allen, B., Plane, J. M. C., Heard, D. E., Lee, J. D., Pilling, M. J. and Kulmala, M. 1999. On the photochemical production of new particles in the coastal boundary layer. *Geophys. Res. Letts.* **26**, 1707–1710.

Pandis, S. N., Paulson, S. E., Seinfeld, J. H. and Flagan, R. C. 1991. Aerosol formation in the photooxidation of isoprene and b-pinene. *Atm. Environ.* **25A**, 997–1008.

Pirjola, L. 1999. Effects of the increased UV radiation and biogenic VOC emissions on ultrafine aerosol formation, *J. Aerosol. Sci.* **30**, 355–367.

Pirjola, L. and Kulmala, M. 1998. Modelling the formation of H_2SO_4–H_2O particles in rural, urban and marine conditions. *Atmos. Res.* **46**, 321–347.

Pirjola, L., Kulmala, M., Wilck, M., Bischoff, A., Stratmann, F. and Otto, E. 1999. Effects of aerosol dynamics on the formation of sulphuric acid aerosols and cloud condensation nuclei. *J. Aerosol Sci.* **30**, 1079–1094.

Pitchford, M. L. and McMurry, P. H. 1994. Relationship between measured water vapor growth and chemistry of atmospheric aerosol for Grand Canyon, Arizona, in winter 1990. *Atmos. Environ.* **28**, 827–839.

Reid, R. C., Prausnitz, J. M. and Poling, B. E. 1987. The Properties of Gases and Liquids, 4 th edition. McGraw-Hill, New York, 741 pp.

Saxena, P and Hildemann, L. M. 1996. Water-soluble organics in atmospheric particles: A critical review of the literature and application of thermodynamics to identify candidate compounds. *J. Atmos. Chem.* **24**, 57–109.

Saxena P. and Hildemann L. M. 1997. Water absorption by organics: Survey of laboratory evidence and evaluation of UNIFAC for estimating water activity. *Environ. Sci. Technol.* **31**, 3318–3324.

Schack Jr., C. J., Pratsinis, S. E. and Friedlander, S. K. 1985. A general correlation for deposition of suspended particles from turbulent gases to completely rough surfaces. *Atmos. Environ.* **19**, 953–960.

Simpson, D. 1992. Long-period modelling of photochemical oxidants in Europe. Model calculation for July 1985. *Atmos. Environ.* **26A**, 1609–1634.

Tao, Y. and McMurry, P. H. 1989. Vapour pressures and surface free energies of C_{14}–C_{18} monocarboxylic acids and C_5-dicarboxylic and C_6-dicarboxylic acids. *Environ. Sci. Technol.* **23**, 1519–1523.

Valkama, I., Salonoja, M., Toivonen, H., Lahtinen, J. and Pöllänen, R. 1995. Transport of Radioactive Gases and Particles from the Chernobyl Accident. In: Environmental Impact of Radioactive Releases. IAEA-SM-339/69. International Atomic Energy Agency, Vienna, 57–69.

Vesala, T., J. Haataja, P. Aalto, N. Altimir, G. Buzorius, E. Garam, K. Hämeri, H. Ilvesniemi, V. Jokinen, P. Keronen, T. Lahti, T. Markkanen, J. M. Mäkelä, E. Nikinmaa, S. Palmroth, L. Palva, P. Pohja, J. Pumpanen, U. Rannik, E. Siivola, H. Ylitalo, P. Hari, and M. Kulmala 1998. Long-term field measurements of atmosphere-surface interactions in boreal forest combining forest ecology, micrometeorology, aerosol phys-

ics and atmospheric chemistry, *Trends in Heat, Mass & Momumtum Transfer* **4**, 17–35.

Weber, R. J., McMurry, P. H., Mauldin, R. L., Tanner, D., Eisele, F. L., Brechtel, F., Kreidenweis, S., Kok, G., Schillawski, R. and Baumgardner, D. 1998. A study of new particle formation and growth involving biogenic trace gas species measured during ACE-1. *J. Geophys. Res.* **103**, 16385–16396.

Weber, R. J., McMurry, P. H., Mauldin, R. L., Tanner, D., Eisele, F. L.,Clarke, A. D. and kapustin, V. 1999. New particle formation in the remote troposphere: A comparison of observations at various sites. *Geophys. Res. Lett*. **26**, 307–310.

Viisanen, Y., Kulmala, M. and Laaksonen, A. 1997. Experiments on gas-liquid nucleation of sulfuric acid and water. *J. Chem. Phys.* **107**, 920–926.

Virkkula, A., Van Dingenen, R., Raes, F. and Hjorth, J. 1999. Hygroscopic properties of aerosol formed by oxidation of limonene, a-pinene and b-pinene. *J. Geophys. Res.* **104**, 3569–3579.

Wilemski, G. 1984. Composition of the critical nucleus in multicomponent vapor nucleation. *J. Chem. Phys.* **80**, 1370–1372.